scientific reports

Check for updates

OPEN

Activation of peroxymonosulphate using a highly efficient and stable $ZnFe_2O_4$ catalyst for tetracycline degradation

Xuying Zhao[1,5], Wei Li[2,5], Junyi Gao[3,5], Caibin Li[3], Yansong Xiao[4], Xue Liu[1], Dean Song[1]✉ & Jiguang Zhang[1]✉

Tetracycline (TC) is a widely used antibiotic that adversely affects ecosystems and, therefore, must be removed from the environment. Owing to their strong ability to oxidise pollutants, including antibiotics, and selectivity for these pollutants, an improved oxidation method based on sulphate radicals (SO4·⁻) has gained considerable interest. In this study, a novel technique for removing TC was developed by activating peroxymonosulphate (PMS) using a $ZnFe_2O_4$ catalyst. Using the co-precipitation method, a $ZnFe_2O_4$ catalyst was prepared by doping zinc into iron-based materials, which increased the redox cycle, while PMS was active and facilitated the production of free radicals. According to electron paramagnetic resonance spectroscopy results, a $ZnFe_2O_4$ catalyst may activate PMS and generate $SO_4·^-$, HO·, $O_2·^-$, and $^1O_2$ to eliminate TC. This research offers a new method for creating highly effective heterogeneous catalysts that can activate PMS and destroy antibiotics. The study proposes the following degradation pathways: hydroxylation and ring-opening of TC based on the products identified using ultra-performance liquid chromatography-mass spectrometry. These results illustrated that the prepared $ZnFe_2O_4$ catalyst effectively removed TC and exhibited excellent catalytic performance.

Recently, due to the rapid development of industry, more and more antibiotic pollutants are discharged into the water body, resulting in increasingly serious water pollution. Tetracycline (TC) is a widely used antibiotic in medical and livestock farming[1]. However, a significant amount of TC is released into the environment and is not absorbed by humans or animals, resulting in increased microbial resistance and harmful impacts on ecological system[2,3]. TC levels as high as 20 mg/L have been reported in aquaculture wastewater, and recently, TC has been detected in drinking water[4,5]. Therefore, effective methods for the removal of TC from aqueous solutions have become a matter of urgent concern.

In recent years, antibiotics have been removed from water using various methods such as adsorption, biodegradation[6], photodegradation[7,8], and advanced oxidation processes (AOPs)[9]. The conventional methods such as adsorption and membrane processes often have some limitations including production of secondary pollutants, high cost and tedious process. The use of AOPs, in which large organic molecules are converted into small organic molecule compounds and even H_2O and CO_2, is the most effective method for removing TC[10,11]. Advanced oxidation process based on peroxymonosulfate (PMS) activation emerged as one of the most promising technologies for antibiotics remediation.

$SO_4·^-$ has a higher oxidation potential, longer duration, and wider pH range compared to HO· produced via the Fenton reaction[12]. Generally, persulfates such as PMS or peroxydisulfate (PDS) are used to produce $SO_4·^-$[13–15]. PMS with an asymmetric structure exhibits a stronger oxidation performance than PDS with a solid symmetric framework[16]. Therefore, PMS is widely used in radical sulphate-based AOPs, which are typically facilitated by using metal-containing catalysts (Co, Fe, Cu, and Mn)[17–22]. However, highly effective, reliable, and recyclable heterogeneous catalysts for practical applications are still required. Heterogeneous catalyst is preferred as PMS activator compared to homogeneous catalyst due to the ease of catalyst recovery, minimum release of secondary pollutant and the potential to operate under such extreme conditions (high pressure and high temperature).

[1]Institute of Tobacco Research, Chinese Academy of Agricultural Sciences, Qingdao 266101, China. [2]China Tobacco Jiangsu Industrial Co., Ltd., Nanjing 210019, China. [3]Bijie Tobacco Branch Company of Guizhou Province, Bijie 551700, China. [4]Chenzhou Tobacco Company of Hunan Province, Chenzhou 423000, China. [5]These authors contributed equally: Xuying Zhao, Wei Li and Junyi Gao. ✉email: songdean@caas.cn; zhangjiguang@caas.cn

Among the transition-metal-based catalysts, Fe-based catalysts are frequently utilised to trigger PMS because of their high effectiveness, safety, non-toxicity, and low price. Fe-based catalysts that can activate PMS to breakdown organic pollutants include magnetic Fe_3O_4, α-Fe_2O_3, γ-Fe_2O_3, and δ-FeOOH[23]. Although low valence Fe^{2+} and Fe^0 are readily oxidised, the slow cycle of Fe^{2+}/Fe^{3+} results in low PMS activation efficiency[24]. Therefore, to eliminate these negative effects, bimetallic oxide catalysts have been proposed as substitutes for improving catalytic activity and stability. In the past, there were many studies on the degradation of organic pollutants by persulfate using Fe–Mn, Fe–C_O bimetallic oxides as catalysts[20,22,24], but the leaching of C_O and Mn ions will cause secondary pollution to the environment, therefore, this study focused on environmental pollution-free Fe–Zn bimetallic oxide catalysts.

In this study, $ZnFe_2O_4$ catalyst was synthesised using the co-precipitation reaction, and its performance in TC degradation was evaluated. The primary goals of this study were to (1) investigate the physicochemical characteristics of the catalyst and discuss its catalytic effectiveness in PMS systems, (2) investigate the effect of various environmental conditions on TC degradation, and (3) examine the reactive oxygen species generated in the $ZnFe_2O_4$/PMS system and elucidate the TC degradation process. Our study provides a new perspective on finding improved, inexpensive, and eco-friendly catalysts.

Methods

Materials. PMS ($KHSO_5{\cdot}0.5KHSO_4{\cdot}0.5K_2SO_4$), iron hexahydrate chloride ($FeCl_3{\cdot}6H_2O$), zinc chloride ($ZnCl_2$), TC, sodium chloride (NaCl), sodium carbonate (Na_2CO_3), and sodium dihydrogen phosphate (NaH_2PO_4) were supplied by Aladdin Industrial Co., Ltd. Hydrochloric acid (HCl), ethanol, and sodium hydroxide (NaOH) were purchased from Guangzhou Chemical Reagent Co. Deionied water (DI) was used throughout the experiment. All reagents were of the lowest analytical quality.

Synthesis of $ZnFe_2O_4$. Using a co-precipitation method, $ZnFe_2O_4$ was synthesised. First, $FeCl_3{\cdot}6H_2O$ and $ZnCl_2$ were ultrasonically dispersed in 50 mL of DI water for 30 min. The resultant mixture was then placed in a water bath at 50 °C and stirred magnetically. NaOH was added to the solution until the pH reached 9, and the suspension was continuously stirred and maintained at 50 °C for 1 h. The $ZnFe_2O_4$ composites were then centrifuged, separated, and washed with ethanol and ultrapure water to reach a pH of 7. The obtained composites were dried at 60 °C for 24 h, pulverised, passed through an 80-mesh sieve, and then calcined at 600 °C for 2 h under N_2 gas.

Characterization of the catalyst. The X-ray diffraction (XRD) pattern were measured between 5 and 80° at 40 kV and 250 mA. The morphology of the $ZnFe_2O_4$ composites was obtained using scanning electron microscopy (SEM; TESCAN MIRA LMS) equipped with energy-dispersive X-ray spectroscopy (EDS). X-ray photoelectron spectroscopy (XPS) was performed using a Thermo Scientific K-Alpha photoelectron spectrometer system.

Catalytic activity test. To evaluate the catalytic performance and reusability of $ZnFe_2O_4$, we determined its TC removal efficiency. To achieve an equilibrium between adsorption and desorption, the catalyst (0.2 g/L) was uniformly suspended in the TC solution (20 mg/L) at 25 °C and continuously shaken for 30 min. To initiate the catalytic oxidation, PMS was introduced into the reaction solution. We collected 2 mL of sample solutions at a time, filtered them through a 0.22 mm membrane, and measured their TC content using an ultraviolet–visible spectrophotometer at 360 nm. An ultra-performance liquid chromatography-mass spectrometry (UPLC-MS) system was used to identify the TC oxidation intermediates. Reactive oxygen species (ROS) were detected using electron paramagnetic resonance (EPR). After the reaction, the catalyst was collected, washed with ethanol and water, and used in a subsequent cycle to determine its suitability for reuse.

Results and discussion

Characterization of catalysts. The XRD pattern of the prepared catalyst matched that of cubic spinel $ZnFe_2O_4$ (JCPDS file No. 22-1012), indicating the presence of $ZnFe_2O_4$ crystals (Fig. 1). Six diffraction peaks were observed at $2\theta = 18.19°$, 29.92°, 35.26°, 42.84°, 45.45°, and 62.21°, which corresponded to the (111), (220), (311), (400), (511), and (440) planes of the $ZnFe_2O_4$, respectively, indicating its high surface purity and good crystallinity.

The SEM was used to examine the surface morphology and particle size distribution of $ZnFe_2O_4$. Figure 2 shows an SEM image of a synthetic $ZnFe_2O_4$ catalyst at various magnifications. Evidently, $ZnFe_2O_4$ nanoparticles with hexagonal and spherical structures are uniformly dispersed. After the reaction, the surface pores of the catalyst become larger.The homogenous distribution of the $ZnFe_2O_4$ particles may help in establishing contact between the catalyst and oxidant, facilitating the activation of PMS[25]. Moreover, the surface of $ZnFe_2O_4$ contains several pores, which help adsorb TC on the catalyst surface.

TC degradation in various systems. The degradation of tetracycline under different Fe-based catalysts was illustrated in Table 1. TC removal efficiency was higher (63%) than other Fe-based catalysts, when Fe–Zn catalysts was employed in the same reaction conditions. So, the TC removal efficiencies were investigated in various systems to evaluate the catalytic effectiveness of $ZnFe_2O_4$-activated PMS for TC degradation (Fig. 3a). $ZnFe_2O_4$ alone was found to remove 15% of TC within 30 min because of TC adhering to the large surface area of the catalyst. Despite being a powerful oxidant (E = 1.82 V), PMS alone could remove only 30% of the TC in a 60-min period due to insufficient catalyst for PMS activation and oxygen radical production. The TC removal

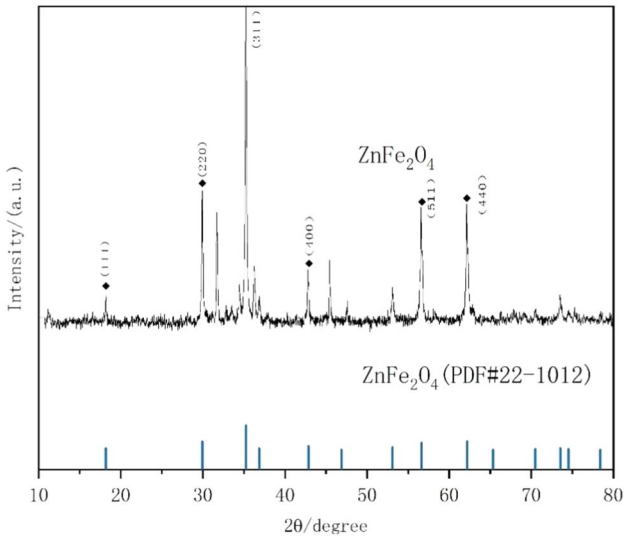

Figure 1. X-ray diffraction pattern of the synthesized $ZnFe_2O_4$ catalyst.

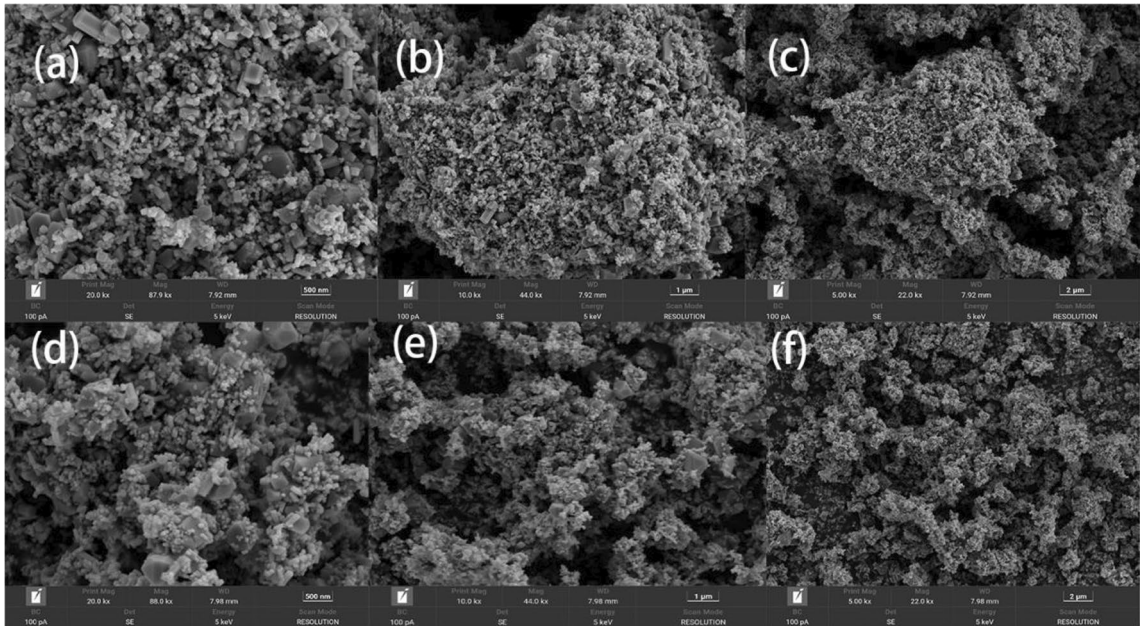

Figure 2. SEM images of $ZnFe_2O_4$ particles before and after the reaction. Higher magnification suggests the presence of agglomerated nanoparticles.

Catalyst (Dose, g/L)	PMS (g/L)	Pollutants	Degradation efficiency (%)	Reaction time (min)
Fe–Sn (0.1)	0.1	TC (20 mg/L)	56	60
Fe–Cu (0.1)	0.1	TC (20 mg/L)	44	60
Fe–Al (0.1)	0.1	TC (20 mg/L)	58	60
Fe–Zn (0.1)	0.1	TC (20 mg/L)	63	60

Table 1. Comparison of performance of different Fe-based catalysts.

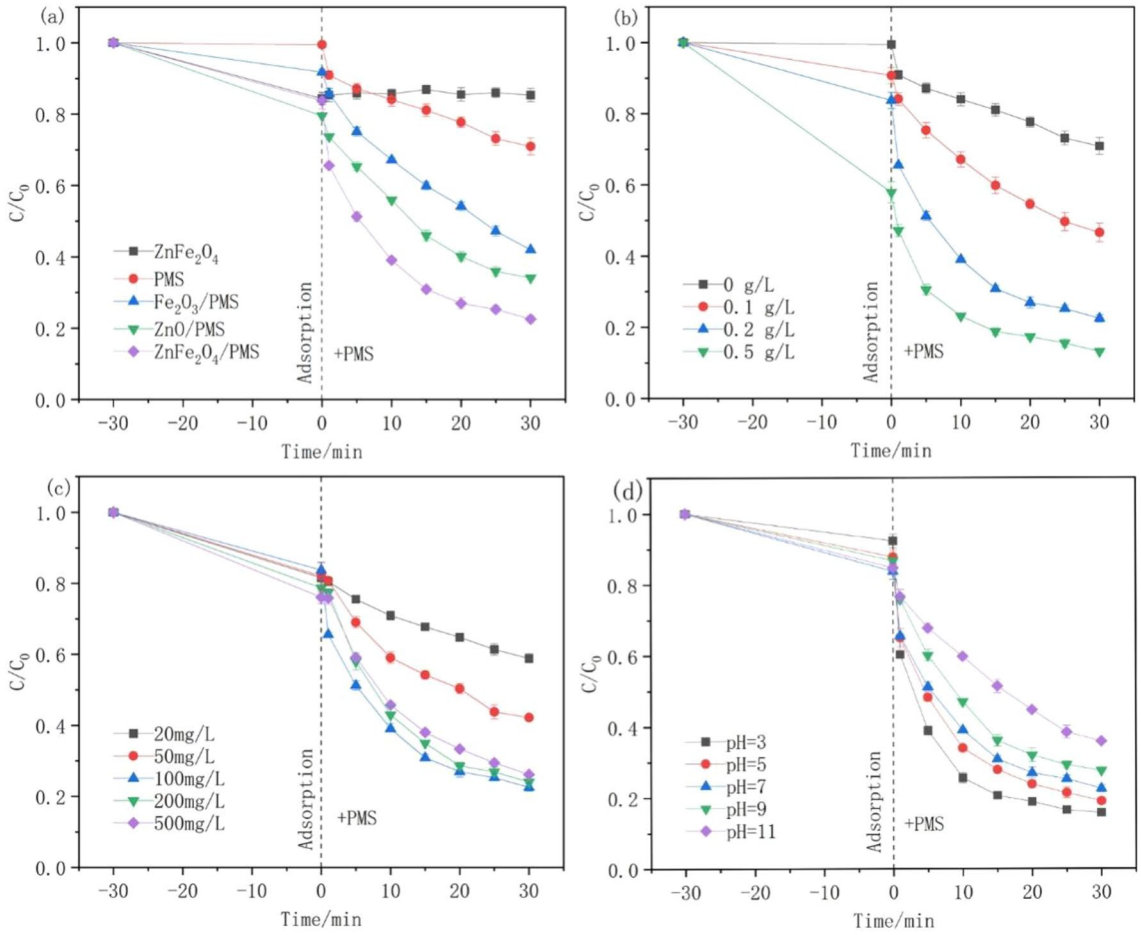

Figure 3. Effects of (**a**) different catalysts, (**b**) catalyst dosage, (**c**) PMS dosage, (**d**) initial pH on TC degradation (Unless stated, [Catalyst] = 200 mg L^{-1}, [TC] = 20 mg L^{-1}, [PMS] = 100 mg L^{-1}, pH = 7).

efficiencies of Fe_2O_3 and ZnO as catalysts were 60% and 66%, respectively, demonstrating that both ZnO and Fe_2O_3 can activate PMS. However, the TC degradation efficiency could reach 78% in $ZnFe_2O_4$/PMS system, indicating its improved catalytic performance.

Catalytic activity and reaction parameter effects. The effects of the catalyst amount, PMS addition amount, and starting pH on TC decomposition were investigated to determine the catalytic oxidation efficiency of $ZnFe_2O_4$. The TC degradability improved as the catalyst quantity was increased from 0.1 to 0.5 g L^{-1}, as shown in Fig. 3b. With a catalyst concentration of 0.1 g L^{-1}, 53% TC was removed in 60 min. This is attributed to the increased number of active sites available for PMS activation as the catalyst dose increases to facilitate TC degradation[26]. When the catalyst concentration was increased to 0.2 g L^{-1}, TC removal increased to 78% in 60 min. However, no discernible improvement was observed on further increasing the catalyst amount to 0.5 g L^{-1}, which may be attributed to the ability of the catalyst to bind excess radicals that tend to aggregate[27–30]. Figure 3c shows the effect of the PMS concentration on the TC removal efficiency. Using 20 mg L^{-1} PMS, the TC elimination was 42% within 60 min and reached to 78% when using 100 mg L^{-1} PMS. This could be because increasing the PMS concentration increases the contact between PMS and the catalyst, thus producing more free radicals[31]. Nevertheless, the effectiveness of TC elimination decreased when the PMS concentration was increased further. Because the excess PMS could quench $SO_4{\cdot}^-$ and HO· to form $SO_5{\cdot}^-$ (Eqs. 1 and 2) with weak oxidation ability[32], the produced $SO_4{\cdot}^-$ or $SO_5{\cdot}^-$ should also have a self-quenching ability (Eqs. 3 and 4)[33–36]. Therefore, in future studies, 100 mg/L PMS should be used as the optimal concentration.

$$HSO_5^- + SO_4{\cdot}^- \rightarrow SO_5{\cdot}^- + H^+ + SO_4^{2-} \quad (1)$$

$$HSO_5^- + HO{\cdot} \rightarrow SO_5{\cdot}^- + H_2O \quad (2)$$

$$SO_4{\cdot}^- + SO_4{\cdot}^- \rightarrow S_2O_8^{2-} \quad (3)$$

$$SO_5 \cdot^- + SO_5 \cdot^- \rightarrow S_2O_8^{2-} + O_2 \quad (4)$$

A key factor influencing TC removal is the initial pH of the reaction solution. Figure 3d shows that the TC removal efficiencies within 60 min were 85%, 81%, 78%, 73%, and 64% at different pH values of 3.0, 5.0, 7.0, 9.0, and 11.0, respectively. According to these findings, $ZnFe_2O_4$-activated PMS could dissolve PMS over a broad pH range, and its removal effectiveness decreased with increasing pH. Generally, SO4·$^-$, which can be manufactured in large quantities for TC degradation, is the primary active species under acidic conditions (Eqs. 5 and 6)[37,38]. However, $SO_4 \cdot^-$ tends to react with OH^- to form HO· under alkaline conditions (Eq. 7)[39]. To dissociate TC chemical bonds, the oxidative potential of the HO· radical should be smaller than that of the $SO_4 \cdot^-$ radical. A higher concentration of OH^- can also cause HO· to interact with OH^-, resulting in radical annihilation and reduced TC degradation efficiency.

$$S_2O_8^{2-} + H^+ \rightarrow HS_2O_8^- \quad (5)$$

$$HS_2O_8^- \rightarrow SO_4 \cdot^- + SO_4 \cdot^- + H^+ \quad (6)$$

$$SO_4 \cdot^- + OH^- \rightarrow SO_4^{2-} + HO \cdot \quad (7)$$

Effects of different anions on TC degradation. Water and wastewater contain various inorganic anions that affect tetracycline removal. Therefore, the effects of Cl^-, CO_3^{2-}, and $H_2PO_4^-$ on the rate of TC degradation in the $ZnFe_2O_4$/PMS system were studied. Figure 4a shows that 1 mM of Cl^- had a slight effect on TC degradation; however, 5–10 mM of Cl^- could improve TC removal efficiency to 87%. Furthermore, high levels of Cl^- may transfer electrons to PMS, resulting in sulphate radicals and superabundant chlorine species (Eqs. 8 and 9)[40–43], which may participate in the TC degradation process[44].

$$Cl^- + ROS \rightarrow Cl \cdot \quad (8)$$

$$Cl \cdot + HSO_5^- \rightarrow SO_4 \cdot^- + HOCl \quad (9)$$

Moreover, increasing the CO_3^{2-} concentration from 1 to 10 mM facilitated TC breakdown (Fig. 4b). This might be attributed to the activation of asymmetrically structured PMS by CO_3^{2-}, thus producing more reactive free radicals (Eq. 10)[45–47].

$$CO_3^{2-} + HSO_5^- + H^+ \rightarrow SO_4 \cdot^- + 2OH^- + CO_2 \quad (10)$$

Similarly, Fig. 4c shows that $H_2PO_4^-$ degrades TC rapidly, which may be due to the transformation of $SO_4 \cdot^-$ into the more reactive $H_2PO_4 \cdot^-$ as shown in(Eqs. 11 and 12)[48].

$$SO_4 \cdot^- + H_2PO_4^- \rightarrow SO_4^{2-} + H_2PO_4 \cdot^- \quad (11)$$

$$HO \cdot + H_2PO_4^- \rightarrow OH^- + H_2PO_4 \cdot^- \quad (12)$$

Reusability of $ZnFe_2O_4$ in catalytic reaction. The most crucial factor in practical applications is the capacity of the catalyst to be reused. To investigate the reusability of $ZnFe_2O_4$, four cycling runs were performed under ideal experimental conditions. As shown in Fig. 5, the TC degradation efficiencies reduced from 77 to 66% in 60 min after 4 cycles, indicating the good reusability of the $ZnFe_2O_4$ catalyst. A minor metal ion overflow on the catalyst may have decreased its activity. Furthermore, TC decomposition may have been hampered by intermediate products absorbed by the catalyst[49].

Catalytic mechanism. To explore the catalytic mechanism of $ZnFe_2O_4$, ROS involved in the $ZnFe_2O_4$/PMS system were investigated using EPR spectroscopy. DMPO was used to capture $SO_4 \cdot^-$, HO·, and $O_2 \cdot^-$ using spin trapping, and TEMP was used to detect $^1O_2$. As shown in Fig. 6a, the DMPO-HO· and DMPO- $SO_4 \cdot^-$ adducts showed their characteristic peaks when the time was increased from 0 to 10 min. Moreover, the DMPO-$O_2 \cdot^-$ adduct signal in Fig. 6b indicates that $O_2 \cdot^-$ may also be involved in TC degradation. Moreover, the TEMP-$^1O_2$ adduct signal was detected at 10 min, implying the presence of $^1O_2$ in the reaction (Fig. 6c). These findings demonstrated that PMS might be triggered by $ZnFe_2O_4$ producing some active substance that removes TC.

XPS was used to analyse changes in Zn and Fe valence states in untreated and treated $ZnFe_2O_4$ catalysts to further investigate their role in PMS activation. The C 1*s*, O 1*s*, Fe 2*p*, and Zn 2*p* peaks of both new and used catalysts in Fig. 7 indicate the good stability of $ZnFe_2O_4$. The peaks at 284.8, 530.8, 711.5, and 1021.6 eV in Fig. 7a correspond to C 1*s*, O 1*s*, Fe 2*p*, and Zn 2*p*, respectively. Table 2 shows the relative element contents before and after the reaction. The C 1*s* orbital in the samples before and after the reaction has similar components, which can be identified as C–O, C–C, O=C–O, and C=O based on the peak patterns and binding energies of 286.3, 284.8, 288.9, and 287.2 eV, respectively (Fig. 7b and Table 3). In Fig. 7c, the energy difference between the spin–orbit splitting peaks (2*p*3/2 and 2*p*1/2) is approximately 23 eV, and the spectral peak area ratio (2*p*3/2:2*p*1/2) is approximately 2:1. The energy position of Zn 2*p* spectral peaks and the database suggest that 1021.9 eV should

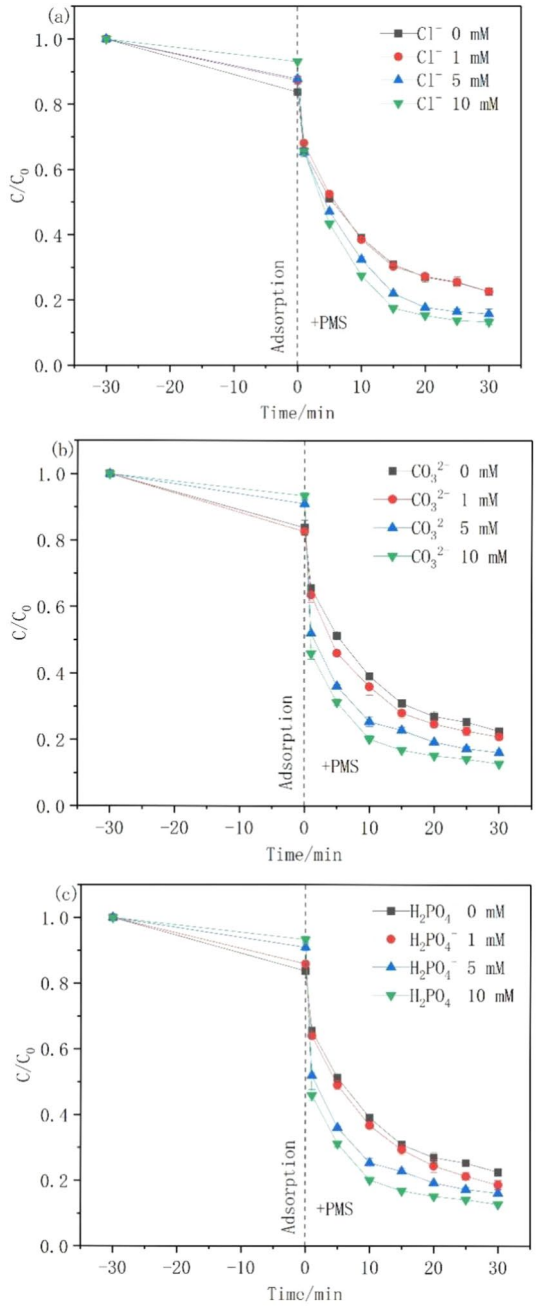

Figure 4. Effects of co-existing (**a**) chloride, (**b**) carbonate, and (**c**) phosphate ions on TC degradation ([Catalyst] = 200 mg L^{-1}, [TC] = 20 mg L^{-1}, [PMS] = 100 mg L^{-1}, pH = 7).

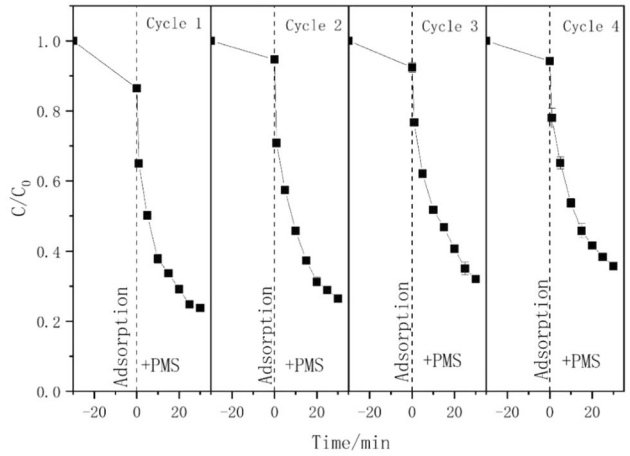

Figure 5. TC degradation in four successive operation catalyzed by $ZnFe_2O_4$. ([Catalyst] = 200 mg L^{-1}, [TC] = 20 mg L^{-1}, [PMS] = 100 mg L^{-1}, pH = 7).

correspond to ZnO. Based on the Fe 2*p* spectrum in Fig. 7d, the Fe species in the catalyst should be Fe^{3+} with the lowest peak intensity at 708.9 eV. The peaks at 714.5 and 719.3 eV are surface and satellite peaks of the catalyst, respectively, whereas those at 710.0, 711.0, 712.0, and 713.0 eV correspond to the four typical multiple cleavages of Fe^{3+} with relative contents listed in Table 4. Based on these results, the valence states of Fe and Zn in the catalyst have not changed substantially. However, following the reaction, the carbon content rose, whereas the concentrations of Fe and Zn decreased. Although the catalyst contains only Fe^{3+}, its content at a low binding energy increased after the reaction.

Degradation pathways of TC. To elucidate the TC decomposition process, the main products were qualitatively analysed using the ESI Q Orbitrap HRMS. Figure 8 shows the possible degradation pathways discussed below. The initial compound (TC) has an ion peak at *m/z* 445, corresponding to the proton-ionised form of $[M+H]^+$. The first possible reaction pathway involves the formation of the *m/z* 461 product via oxidative hydroxylation of the "A" ring of TC, *m/z* 477 via hydroxylation of the "D" ring, and *m/z* 449 via oxidative "D" ring opening and removing the carbonyl group. Further oxidation could occur when the C–C bonds are broken and side chains are removed to yield *m/z* 378 and 394. In addition, *m/z* 366 could be obtained via the oxidative ring opening of the "B" ring. The second possible reaction pathway involves the formation of product *m/z* 461 via hydroxylation of the "D" ring, product *m/z* 495 via the "D" ring opening, and products *m/z* 376 and 422 via oxidative breaking of the C–C bonds. The product *m/z* 366 was then obtained by oxidising the "B" ring and removing the carboxyl group. The third possible reaction channel involves the TC breakdown via the C–N bond and demethylation of dimethylamine to procure *m/z* 431, the hydroxylation of the "A" ring of TC to obtain *m/z* 463, and the oxidative opening of the "D" ring to procure *m/z* 364. The splitting of the rings to form tiny molecules of acids and amines, as well as H_2O, CO_2, NO_3^-, and NH_4^+, indicate oxidative breakdown and complete degradation of the compounds.

Conclusions

The co-precipitation method was used to synthesise a highly active $ZnFe_2O_4$ catalyst, which was subsequently used as a PMS activator to degrade TC. The $ZnFe_2O_4$ catalyst was studied using XRD, SEM, and XPS. The effects of the changes in the amount of catalyst, PMS concentration, and initial pH on TC decomposition efficiency were studied under various conditions. Under the optimised reaction conditions, the TC degradation efficiency reached 78%. Inorganic anions ($H_2PO_4^-$,$H_2PO_4^-$, CO_3^{2-}, and Cl^-) can promote TC degradation to certain extent. In the cyclic experiments, $ZnFe_2O_4$ was found to be catalytically active and stable. In addition, the EPR and XPS results revealed the presence of numerous active substances, including $SO_4^{\cdot-}$, HO·, $O_2^{\cdot-}$, and $^1O_2$, in the TC mineralization process. The potential TC degradation mechanisms of the $ZnFe_2O_4$/PMS system were hypothesised to depend on the products identified by UPLC-MS. These results demonstrated that the prepared $ZnFe_2O_4$ catalyst effectively removed TC and exhibited excellent catalytic performance.

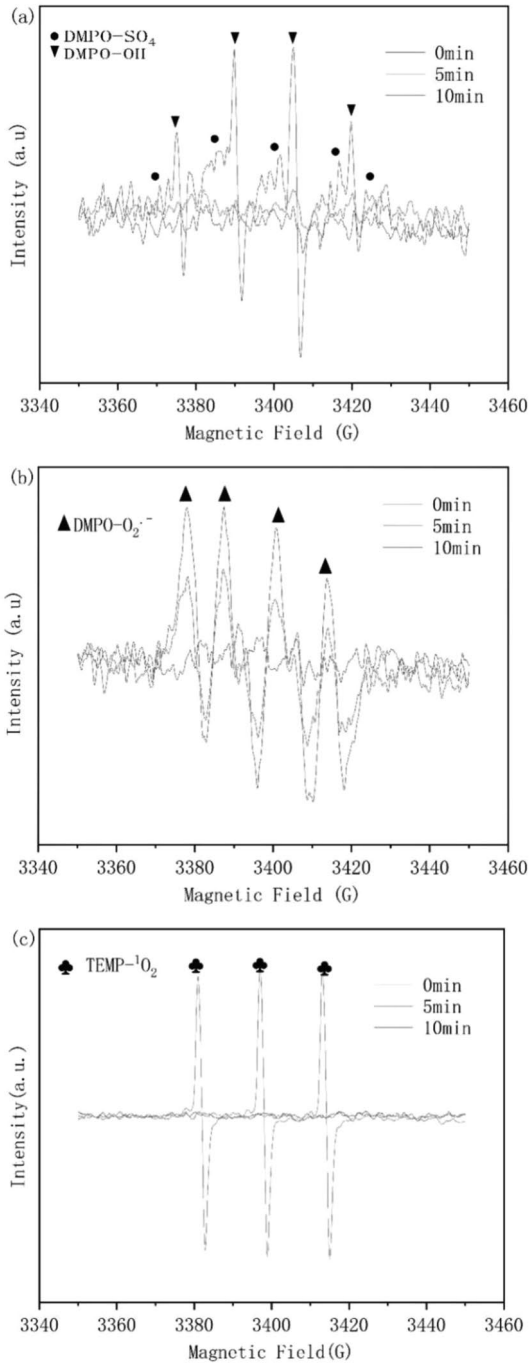

Figure 6. EPR spectroscopy measurements of (**a**) $SO_4^{\cdot -}$ and HO·, (**b**) $O_2^{\cdot -}$ and (**c**) $^1O_2$.

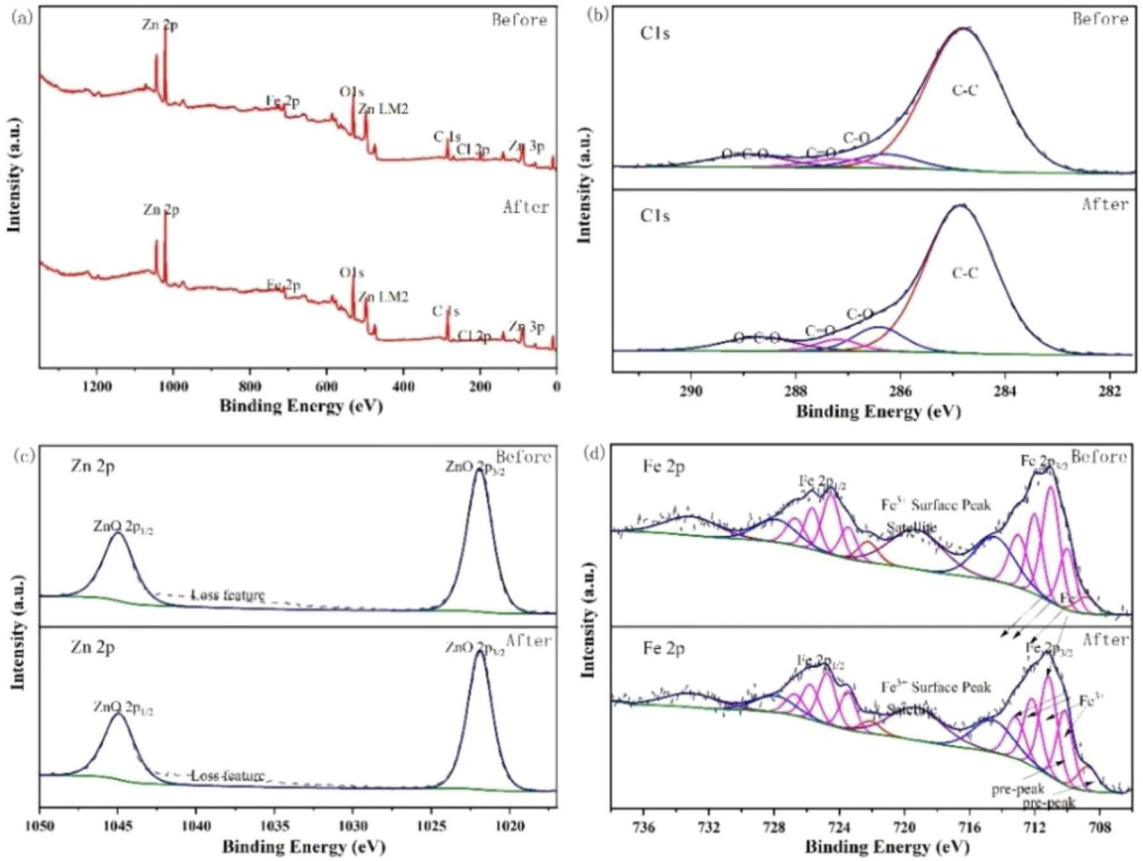

Figure 7. XPS spectra of (**a**) survey, (**b**) C1*s*, (**c**) Zn 2*p*, (**d**) Fe 2*p* for fresh and used $ZnFe_2O_4$ catalyst.

Sample	C	O	Zn	Fe
1	42.96	35.44	13.97	7.63
2	52.09	32.84	9.80	5.27

Table 2. Relative content of the elements in the samples/at.%.

Sample	C–C	C–O	C=O	O=C=O
1	82.03	6.52	4.07	7.38
2	79.22	9.26	3.88	7.64

Table 3. Relative content of each chemical bond of C1s/at.%.

Sample	1-Fe^{3+}	2-Fe^{3+}	3-Fe^{3+}	4-Fe^{3+}
1	18.96	38.70	23.33	19.01
2	24.48	35.37	24.15	16.00

Table 4. Relative content of each chemical bond of Fe^{3+}/at.%.

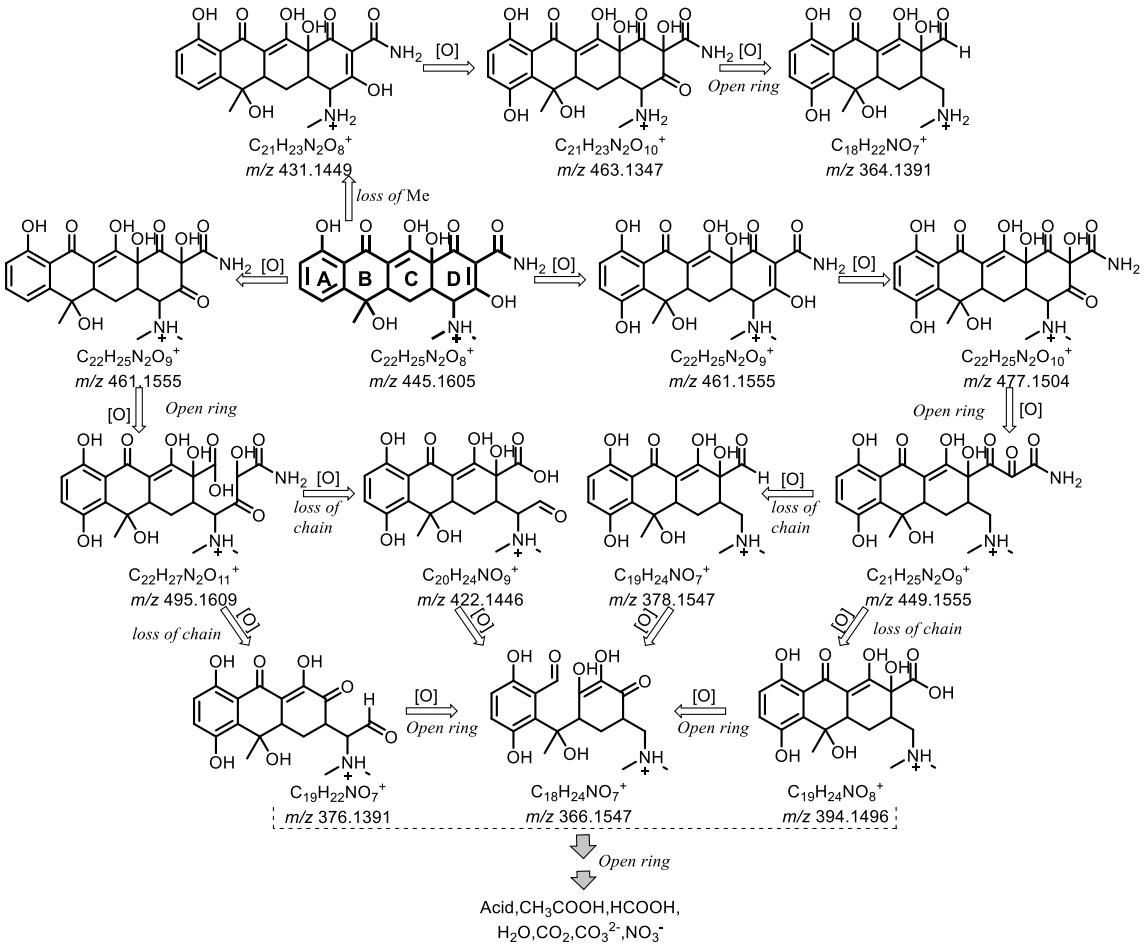

Figure 8. Degradation pathways and proposed mechanism of tetracycline.

Data availability

Data is available under reasonable request to the corresponding author.

Received: 27 March 2023; Accepted: 18 July 2023
Published online: 25 August 2023

References

1. Kovalakova, P. *et al.* Occurrence and toxicity of antibiotics in the aquatic environment: A review. *Chemosphere* **251**, 126351. https://doi.org/10.1016/j.chemosphere.2020.126351 (2020).
2. He, J. *et al.* Enhanced peroxymonosulfate activation over heterogeneous catalyst $Cu_{0.76}Co_{2.24}O_4$/SBA-15 for efficient degradation of sulfapyridine antibiotic. *Ecotoxicol. Environ. Saf.* **216**, 112189. https://doi.org/10.1016/j.ecoenv.2021.112189 (2021).
3. Le, S. *et al.* V_2O_5 nanodot-decorated laminar C_3N_4 for sustainable photodegradation of amoxicillin under solar light. *Appl. Catal. B Environ.* **303**, 120903. https://doi.org/10.1016/j.apcatb.2021.120903 (2022).
4. Sun, J. *et al.* Synchronous removal of tetracycline and copper (II) over Z-scheme $BiVO_4$/rGO/g-C_3N_4 photocatalyst under visible-light irradiation. *Environ. Sci. Pollut. Res.* **29**, 19148–19164. https://doi.org/10.1007/s11356-021-16996-4 (2022).
5. Wei, J., Han, D., Bi, J. & Gong, J. Fe-doped ilmenite $CoTiO_3$ for antibiotic removal: Electronic modulation and enhanced activation of peroxymonosulfate. *Chem. Eng. J.* **423**, 130165. https://doi.org/10.1016/j.cej.2021.130165 (2021).
6. Yang, P. *et al.* Efficient removal of tetracycline in water by a novel chemical and biological coupled system with non-woven cotton fabric as carrier. *Chin. Chem. Lett.* **32**, 2823–2827. https://doi.org/10.1016/j.cclet.2021.02.028 (2021).
7. Dang, C. *et al.* Pre-accumulation and in-situ destruction of diclofenac by a photo-regenerable activated carbon fiber supported titanate nanotubes composite material: Intermediates, DFT calculation, and ecotoxicity. *J. Hazard. Mater.* **400**, 123225. https://doi.org/10.1016/j.jhazmat.2020.123225 (2020).
8. Ji, H. *et al.* 2D/1D graphitic carbon nitride/titanate nanotubes heterostructure for efficient photocatalysis of sulfamethazine under solar light: Catalytic "hot spots" at the rutile–anatase–titanate interfaces. *Appl. Catal. B Environ.* **263**, 118357. https://doi.org/10.1016/j.apcatb.2019.118357 (2020).
9. Wacławek, S. *et al.* Chemistry of persulfates in water and wastewater treatment: A review. *Chem. Eng. J.* **330**, 44–62. https://doi.org/10.1016/j.cej.2017.07.132 (2017).
10. Hao, S.-M. *et al.* Hollow manganese silicate nanotubes with tunable secondary nanostructures as excellent fenton-type catalysts for dye decomposition at ambient temperature. *Adv. Func. Mater.* **26**, 7334–7342. https://doi.org/10.1002/adfm.201603315 (2016).
11. Zhu, L. *et al.* Designing 3D-MoS_2 sponge as excellent cocatalysts in advanced oxidation processes for pollutant control. *Angew. Chem.-Int. Ed.* **59**, 13968–13976. https://doi.org/10.1002/anie.202006059 (2020).
12. Chen, F. *et al.* Catalytic degradation of ciprofloxacin by a visible-light-assisted peroxymonosulfate activation system: Performance and mechanism. *Water Res.* https://doi.org/10.1016/j.watres.2020.115559 (2020).

13. Chen, C. *et al.* In-situ pyrolysis of Enteromorpha as carbocatalyst for catalytic removal of organic contaminants: Considering the intrinsic N/Fe in Enteromorpha and non-radical reaction. *Appl. Catal. B* **250**, 382–395. https://doi.org/10.1016/j.apcatb.2019.03.048 (2019).
14. Jia, M. *et al.* Magnetic heterojunction of oxygen-deficient Ti_3–TiO_2 and Ar-Fe_2O_3 derived from metal-organic frameworks for efficient peroxydisulfate (PDS) photo-activation. *Appl. Catal. B-Environ.* https://doi.org/10.1016/j.apcatb.2021.120513 (2021).
15. Zhang, L.-S. *et al.* carbon nitride supported high-loading Fe single-atom catalyst for activating of peroxymonosulfate to generate O-1(2) with 100% selectivity. *Angew. Chem.-Int. Ed.* **60**, 21751–21755. https://doi.org/10.1002/anie.202109488 (2021).
16. Wang, L. *et al.* Fabrication of Co_3O_4-Bi_2O_3-Ti catalytic membrane for efficient degradation of organic pollutants in water by peroxymonosulfate activation. *J. Colloid Interface Sci.* **607**, 451–461. https://doi.org/10.1016/j.jcis.2021.08.086 (2022).
17. Abdul Nasir Khan, M. *et al.* Metal-organic framework-derived hollow Co_3O_4/carbon as efficient catalyst for peroxymonosulfate activation. *Chem. Eng. J.* **363**, 234–246. https://doi.org/10.1016/j.cej.2019.01.129 (2019).
18. Asif, M. B., Kang, H. & Zhang, Z. Gravity-driven layered double hydroxide nanosheet membrane activated peroxymonosulfate system for micropollutant degradation. *J. Hazard. Mater.* **425**, 127988. https://doi.org/10.1016/j.jhazmat.2021.127988 (2022).
19. Chen, X. *et al.* PMS activation by magnetic cobalt-N-doped carbon composite for ultra-efficient degradation of refractory organic pollutant: Mechanisms and identification of intermediates. *Chemosphere* **287**, 132074. https://doi.org/10.1016/j.chemosphere.2021.132074 (2022).
20. Li, Y. *et al.* Peroxymonosulfate activation on $FeCo_2S_4$ modified g-C3N4 ($FeCo_2S_4$-CN): Mechanism of singlet oxygen evolution for nonradical efficient degradation of sulfamethoxazole. *Chem. Eng. J.* **384**, 123361. https://doi.org/10.1016/j.cej.2019.123361 (2020).
21. Sun, J. A., Wang, L., Wang, Y., Lv, W. & Yao, Y. Activation of peroxymonosulfate by MgCoAl layered double hydroxide: Potential enhancement effects of catalyst morphology and coexisting anions. *Chemosphere* **286**, 131640. https://doi.org/10.1016/j.chemosphere.2021.131640 (2022).
22. Zhao, G. *et al.* Iron-based catalysts for persulfate-based advanced oxidation process: Microstructure, property and tailoring. *Chem. Eng. J.* https://doi.org/10.1016/j.cej.2020.127845 (2021).
23. Zhao, J. *et al.* Superior performance of ZnCoOx/peroxymonosulfate system for organic pollutants removal by enhancing singlet oxygen generation: The effect of oxygen vacancies. *Chem. Eng. J.* **409**, 128150. https://doi.org/10.1016/j.cej.2020.128150 (2021).
24. Liu, Y., Zhou, A., Gan, Y. & Li, X. Roles of hydroxyl and sulfate radicals in degradation of trichloroethene by persulfate activated with Fe^{2+} and zero-valent iron: Insights from carbon isotope fractionation. *J. Hazard. Mater.* **344**, 98–103. https://doi.org/10.1016/j.jhazmat.2017.09.048 (2018).
25. Guo, B. *et al.* Co_3O_4/CoO ceramic catalyst: Bisulfite assisted catalytic degradation of methylene blue. *Ceram. Int.* **47**, 27617–27623. https://doi.org/10.1016/j.ceramint.2021.06.186 (2021).
26. She, S. *et al.* Reusing warm-paste waste as catalyst for peroxymonosulfate activation toward antibiotics degradation under high salinity condition: Performance and mechanism study. *Chem. Eng. J.* **426**, 131295. https://doi.org/10.1016/j.cej.2021.131295 (2021).
27. Cai, C. *et al.* Efficient degradation of bisphenol A in water by heterogeneous activation of peroxymonosulfate using highly active cobalt ferrite nanoparticles. *J. Hazard. Mater.* **399**, 122979. https://doi.org/10.1016/j.jhazmat.2020.122979 (2020).
28. Luo, J. *et al.* Transforming goat manure into surface-loaded cobalt/biochar as PMS activator for highly efficient ciprofloxacin degradation. *Chem. Eng. J.* **395**, 125063. https://doi.org/10.1016/j.cej.2020.125063 (2020).
29. Nguyen, T.-B. *et al.* Construction of ternary $NiCo_2O_4$/MnOOH/GO composite for peroxymonosulfate activation with enhanced catalytic activity toward ciprofloxacin degradation. *Chem. Eng. J.* **446**, 137326. https://doi.org/10.1016/j.cej.2022.137326 (2022).
30. Zhu, S. *et al.* Magnetic Co/Fe nanocomposites derived from ferric sludge as an efficient peroxymonosulfate catalyst for ciprofloxacin degradation. *Chem. Eng. J.* **432**, 134180. https://doi.org/10.1016/j.cej.2021.134180 (2022).
31. Wu, Z. *et al.* Efficient degradation of tetracycline by persulfate activation with Fe, Co and O co–doped g–C_3N_4: Performance, mechanism and toxicity. *Chem. Eng. J.* **434**, 134732. https://doi.org/10.1016/j.cej.2022.134732 (2022).
32. Cao, J. *et al.* Degradation of tetracycline by peroxymonosulfate activated with zero-valent iron: Performance, intermediates, toxicity and mechanism. *Chem. Eng. J.* **364**, 45–56. https://doi.org/10.1016/j.cej.2019.01.113 (2019).
33. Ghanbari, F., Khatebasreh, M., Mahdavianpour, M. & Lin, K.-Y.A. Oxidative removal of benzotriazole using peroxymonosulfate/ozone/ultrasound: Synergy, optimization, degradation intermediates and utilizing for real wastewater. *Chemosphere* **244**, 125326. https://doi.org/10.1016/j.chemosphere.2019.125326 (2020).
34. Ghanbari, F., Wu, J., Khatebasreh, M., Ding, D. & Lin, K.-Y.A. Efficient treatment for landfill leachate through sequential electrocoagulation, electrooxidation and PMS/UV/$CuFe_2O_4$ process. *Sep. Purif. Technol.* **242**, 116828. https://doi.org/10.1016/j.seppur.2020.116828 (2020).
35. Li, M. *et al.* Exploring degradation mechanism of tetracycline via high-effective peroxymonosulfate catalysts of montmorillonite hybridized CoFe composites and safety assessment. *Chem. Eng. J.* **427**, 130930. https://doi.org/10.1016/j.cej.2021.130930 (2022).
36. Tang, L. *et al.* Enhanced activation process of persulfate by mesoporous carbon for degradation of aqueous organic pollutants: Electron transfer mechanism. *Appl. Catal. B* **231**, 1–10. https://doi.org/10.1016/j.apcatb.2018.02.059 (2018).
37. Hussain, I. *et al.* Insights into the mechanism of persulfate activation with nZVI/BC nanocomposite for the degradation of nonylphenol. *Chem. Eng. J.* **311**, 163–172. https://doi.org/10.1016/j.cej.2016.11.085 (2017).
38. Liu, C. *et al.* Coupling metal–organic frameworks and g-C_3N_4 to derive Fe@N-doped graphene-like carbon for peroxymonosulfate activation: Upgrading framework stability and performance. *Appl. Catal. B Environ.* **255**, 117763. https://doi.org/10.1016/j.apcatb.2019.117763 (2019).
39. Xie, M. *et al.* Cobalt doped g-C_3N_4 activation of peroxymonosulfate for monochlorophenols degradation. *Chem. Eng. J.* **360**, 1213–1222. https://doi.org/10.1016/j.cej.2018.10.130 (2019).
40. Li, C.-X. *et al.* Insights on the pH-dependent roles of peroxymonosulfate and chlorine ions in phenol oxidative transformation. *Chem. Eng. J.* **362**, 570–575. https://doi.org/10.1016/j.cej.2019.01.057 (2019).
41. Long, Y. *et al.* Sulfur-containing iron nanocomposites confined in S/N co-doped carbon for catalytic peroxymonosulfate oxidation of organic pollutants: Low iron leaching, degradation mechanism and intermediates. *Chem. Eng. J.* **404**, 126499. https://doi.org/10.1016/j.cej.2020.126499 (2021).
42. Luo, R. *et al.* Singlet oxygen-dominated non-radical oxidation process for efficient degradation of bisphenol A under high salinity condition. *Water Res.* **148**, 416–424. https://doi.org/10.1016/j.watres.2018.10.087 (2019).
43. Yang, S. *et al.* Rapid removal of tetrabromobisphenol A by α-Fe_2O_3-x@Graphene@Montmorillonite catalyst with oxygen vacancies through peroxymonosulfate activation: Role of halogen and α-hydroxyalkyl radicals. *Appl. Catal. B Environ.* **260**, 118129. https://doi.org/10.1016/j.apcatb.2019.118129 (2020).
44. Zhou, X. *et al.* Tunable S doping from Co_3O_4 to Co_9S_8 for peroxymonosulfate activation: Distinguished Radical/Nonradical species and generation pathways. *Appl. Catal. B Environ.* **282**, 119605. https://doi.org/10.1016/j.apcatb.2020.119605 (2021).
45. Ao, X. *et al.* Degradation of tetracycline by medium pressure UV-activated peroxymonosulfate process: Influencing factors, degradation pathways, and toxicity evaluation. *Chem. Eng. J.* **361**, 1053–1062. https://doi.org/10.1016/j.cej.2018.12.133 (2019).
46. Liu, X., Pei, Y., Cao, M., Yang, H. & Li, Y. Highly dispersed copper single-atom catalysts activated peroxymonosulfate for oxytetracycline removal from water: Mechanism and degradation pathway. *Chem. Eng. J.* **450**, 138194. https://doi.org/10.1016/j.cej.2022.138194 (2022).
47. Wang, J. & Wang, S. Effect of inorganic anions on the performance of advanced oxidation processes for degradation of organic contaminants. *Chem. Eng. J.* **411**, 128392. https://doi.org/10.1016/j.cej.2020.128392 (2021).

48. Wan, Q. *et al.* Peroxymonosulfate activation by bimetallic modified syderolite pellets catalyst for degradation of brominobenzonitrile. *Process. Saf. Environ. Prot.* **165**, 505–513. https://doi.org/10.1016/j.psep.2022.07.052 (2022).
49. Liu, Z., Gao, Z. & Wu, Q. Activation of persulfate by magnetic zirconium-doped manganese ferrite for efficient degradation of tetracycline. *Chem. Eng. J.* **423**, 130283. https://doi.org/10.1016/j.cej.2021.130283 (2021).

Acknowledgements

This work was funded by the National Agricultural Product Quality and Safety Risk Assessment Project (GJFP20220204), Agricultural Science and Technology Innovation Program of China (ASTIP-TRIC06), the Science and Technology Project of Bijie Tobacco Branch Company (2020520500240072, 2023520500240162) and the Science and Technology Project of Chenzhou Tobacco Company of Hunan Province (No. 2019-45).

Author contributions

X.Z. design, experiment, analysis, drafting. W.L. design, experiment, analysis, drafting. J.G. design, analysis, investigation. C.L. analysis, investigation. Y.X. analysis, investigation. X.L. analysis, investigation. D.S. conception, resources, revising. J.Z. conception, funding acquisition, revising.

Competing interests

The authors declare no competing interests.

Additional information

Correspondence and requests for materials should be addressed to D.S. or J.Z.

Reprints and permissions information is available at www.nature.com/reprints.

Publisher's note Springer Nature remains neutral with regard to jurisdictional claims in published maps and institutional affiliations.

Open Access This article is licensed under a Creative Commons Attribution 4.0 International License, which permits use, sharing, adaptation, distribution and reproduction in any medium or format, as long as you give appropriate credit to the original author(s) and the source, provide a link to the Creative Commons licence, and indicate if changes were made. The images or other third party material in this article are included in the article's Creative Commons licence, unless indicated otherwise in a credit line to the material. If material is not included in the article's Creative Commons licence and your intended use is not permitted by statutory regulation or exceeds the permitted use, you will need to obtain permission directly from the copyright holder. To view a copy of this licence, visit http://creativecommons.org/licenses/by/4.0/.

© The Author(s) 2023